Materials Chemistry and Physics 141 (2013) 790–796

Contents lists available at SciVerse ScienceDirect

Materials Chemistry and Physics

journal homepage: www.elsevier.com/locate/matchemphys

Study of microstructure and magnetization reversal mechanism in granular CoCrPt:SiO_2 films of variable thickness

G. Varvaro [a,*], A.M. Testa [a], E. Agostinelli [a], D. Fiorani [a], S. Laureti [a], F. Springer [b], C. Brombacher [b], M. Albrecht [b], L. Del Bianco [a,d], G. Barucca [c], P. Mengucci [c], D. Rinaldi [c]

[a] Istituto di Struttura della Materia, Consiglio Nazionale delle Ricerche, Area della Ricerca Roma1, 00015 Monterotondo Scalo, Roma, Italy
[b] Institute of Physics, Chemnitz University of Technology, D-09107 Chemnitz, Germany
[c] Dipartimento SIMAU, Università Politecnica delle Marche, 60131 Ancona, Italy
[d] Dipartimento di Fisica, Università di Bologna and CNISM, I-40127 Bologna, Italy

HIGHLIGHTS

- Granular CoCrPt/SiO_2 films with different thickness were deposited by magnetron sputtering.
- Microstructural properties were found to change with increasing thickness.
- The magnetization reversal mechanism was investigated at room temperature.
- The importance of coherent magnetization reversal processes increases with increasing the magnetic layer thickness.
- The results were confirmed by numerical micromagnetic simulations.

ARTICLE INFO

Article history:
Received 3 October 2012
Received in revised form
21 March 2013
Accepted 10 June 2013

Keywords:
Multilayers
Microstructure
Magnetic properties
Computer modelling and simulation

ABSTRACT

The effect of the thickness and microstructural features on the switching behaviour of granular CoCrPt:SiO_2 films with perpendicular magnetic anisotropy was investigated. TEM plane view and cross section analysis indicate that, while the very first layers grow as uniform nanograins in close contact, the growth proceeds by formation of well-defined CoCrPt columnar islands (7 nm average size) separated by the silicon oxide, the distance among the islands remaining roughly constant along the whole thickness.

The relation between such non-uniform microstructure and the magnetization reversal mechanism at room temperature was investigated by performing hysteresis loops at variable angle as well as time dependent measurements by using a vector vibrating sample magnetometer. Numerical micromagnetic simulations of the hysteresis loops have been carried out to support the description of the experimental observations. The results showed a coexistence of coherent and incoherent reversal processes, the former being more and more pronounced with increasing the magnetic layer thickness, consistently with the microstructural investigations.

1. Introduction

The great technological potential of nanostructured magnetic materials warrants continued study of their structure/magnetic property relationships. As an example, in magnetic recording media, controlling the easy-axis orientation and intergrain interactions and understanding how these properties are affected by the real structure are necessary steps to realize an advanced magnetic recording medium with optimized signal-to-noise ratio, thermal stability and write-ability requirements [1]. In commercial hard disk drives, the recording layer of the medium consists of a continuous CoCrPt film coupled with a granular thin film made of single-domain CoCrPt grains with perpendicular magnetic anisotropy, separated by Si-oxide [2]. Ideally, the Si-oxide at the grain boundaries should completely prevent the ferromagnetic exchange coupling among neighbouring grains and the magnetization reversal would be consistent with a Stoner–Wohlfarth behaviour (coherent reversal) [3]. In general, in thin films, strong exchange intergrain interactions can arise if grains are in contact, however, the strength of such interactions can greatly vary, depending on the nature of grain boundaries, the presence of a crystalline or amorphous matrix, etc. [4–6]. Furthermore, in real systems the actual quality of grain

* Corresponding author.
E-mail address: gaspare.varvaro@ism.cnr.it (G. Varvaro).

0254-0584/$ – see front matter © 2013 Elsevier B.V. All rights reserved.
http://dx.doi.org/10.1016/j.matchemphys.2013.06.005

isolation, which strongly affects the performance of the recording medium, also depends in a quite complex way on the characteristics of the interlayers and seed-layers used in the complete stacking sequence [7] as well as on the film thickness [8,9].

In the present work, we report on the investigation of magnetization reversal mechanism of granular CoCrPt:SiO_2 films with variable thickness and its correlation with structural (XRD, XRR) and microstructural (TEM) properties. The magnetic study was carried-out by performing hysteresis loops at variable angle as well as time dependent measurements by using a vector vibrating sample magnetometer (vVSM). Numerical micromagnetic simulations of the hysteresis loops were carried out to support the description of the experimental observations.

2. Experimental details

$[(Co_{90}Cr_{10})_{80}Pt_{20}]_{92}$:$(SiO_2)_8$ thin films with a nominal thickness of 7.5, 10 and 17.5 nm (hereafter referred to as ML7.5, ML10 and ML17.5) were deposited by magnetron sputtering on 2.5-inch hard disk HOYA substrates, with a complex underlayer structure – Cr(2.5 nm)/Ru(8 nm)/Ru(12 nm) – aimed to promote a perpendicular anisotropy and good microstructural properties; films were covered by a 4 nm protective overcoat of diamond-like carbon.

Structural and microstructural characterization were carried out by X-ray diffraction (XRD), X-ray reflectivity (XRR) and transmission electron microscopy (TEM) techniques. XRD and XRR measurements were performed by a Bruker D8 Advance diffractometer operating with a Cu-Kα radiation source. The XRR curves were fitted by the Leptos 3.03 simulation program. TEM analysis was carried out by a Philips CM200 electron microscope operating at 200 kV. For TEM cross-sectional and plan-view observations, samples were prepared by the conventional thinning procedure consisting of mechanical polishing by grinding papers, diamond pastes and a dimple grinder. Final thinning was carried out by an ion beam system (Gatan PIPS) using Ar ions at 5 kV.

Magnetic measurements were carried out by using a vector vibrating sample magnetometer (vVSM, ADE-Technologies Model 10) equipped with 4 pick-up coils and an electromagnet, which supplies a maximum field of 2 T.

Micromagnetic simulations of room temperature magnetization loops were performed by numerically solving (finite difference method) the standard Landau–Lifshitz–Gilbert–Langevin equation for the time evolution of the magnetization, using the commercial LLG Micromagnetics Simulator™ [10]. To allow a meaningful comparison with experimental results, material parameters were chosen consistently with experimental values.

Table 1
Experimental FWHM values of the rocking curves obtained from the CoCrPt and Ru (002) peaks.

ID	$FWHM_{CoCrPt}$ [°]	$FWHM_{Ru}$ [°]
ML7.5	12.9 ± 0.1	10.4 ± 0.1
ML10	13.5 ± 0.1	11.7 ± 0.1
ML17.5	12.3 ± 0.1	11.6 ± 0.1

3. Results and discussion

3.1. Structural and microstructural analysis

X-ray diffraction patterns of the samples are shown in Fig. 1. The diffraction pattern of sample ML17.5 shows two well-defined main peaks. The most intense peak, labelled as Ru (002), is due to the underlying dual Ru layer, while the second lower intensity peak is attributed to the (002) reflection of the hexagonal CoCrPt recording layer. The absence of any other Ru or CoCrPt peaks suggests a preferential growth of both layers with the *c*-axis perpendicular to the substrate. For samples ML7.5 and ML10 quite similar XRD patterns were observed, but only the Ru (002) main peak was clearly identified. For these samples, the intensity of the CoCrPt reflection is reduced and appears as a shoulder of the Ru (002) main peak.

The degree of preferential growth along the *c*-axis of CoCrPt and Ru layers is estimated by measuring the full width at half maximum (FWHM) of the corresponding rocking curves. The experimental values obtained by a Lorentzian interpolation of the peaks are reported in Table 1. For each sample, the FWHM values of the CoCrPt and the Ru layers are comparable, suggesting a good epitaxial growth of the magnetic layer on the Ru interlayer. However, FWHM values of 10–12°, slightly larger than those commonly reported in similar systems [11], are observed.

To fully characterize the samples in terms of thickness and roughness of each individual layer, XRR investigations were performed. Fig. 2 shows the experimental XRR data for the three samples with superimposed the corresponding fitted curves. Thickness (th) and surface roughness (σ) of the CoCrPt layer are reported in Table 2; errors of 3% and 10% should be considered for thickness and roughness, respectively. For the three samples the

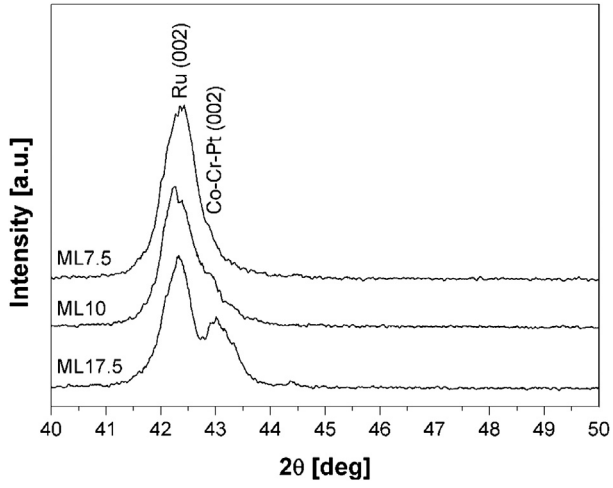

Fig. 1. XRD spectra of sample ML7.5, ML10 and ML17.5.

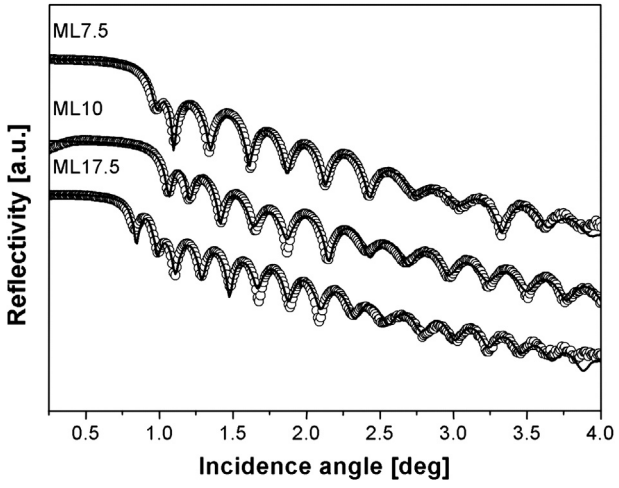

Fig. 2. XRR experimental data (– ○ –) and best fitting (continuous line) for samples ML7.5, ML10 and ML17.5.

Table 2
Best fitted values of thickness (th) and roughness (σ) of the CoCrPt layer.

ID sample	th [nm]	σ [nm]
ML7.5	7.8 ± 0.2	1.0 ± 0.1
ML10	9.2 ± 0.3	1.3 ± 0.1
ML17.5	17.2 ± 0.5	0.7 ± 0.1

thickness estimated by the fitting software (Leptos 3.03) [12] results to be very close to the nominal value. The roughness is comparable for all the three samples and the low values observed indicate that they present a quite smooth surface.

Fig. 3(a–c) shows TEM plan view images of the samples. Fine grains with an average size of 7 nm, well separated by amorphous-like material (Si-oxide), are clearly visible for all samples. The selected area electron diffraction (SAED) pattern of sample ML17.5 is presented in Fig. 3(d). The sequence of the rings in the SAED pattern confirmed the preferential (002) texture of the CoCrPt layer, while the uniform intensity of the rings indicated a random distribution of the CoCrPt grains orientation around the *c*-axis. The SAED patterns of the samples ML7.5 and ML10 revealed a similar ring intensity and geometry.

Both TEM diffraction and X-ray data were used to estimate the lattice parameters of the hexagonal CoCrPt compound. Values of $a = (0.257 \pm 0.003)$ nm and $c = (0.420 \pm 0.003)$ nm are obtained in agreement with values expected for a 20% at. Pt content.

It is worth to note that the TEM plan view observations did not reveal any appreciable difference in the structure of the three analysed samples. However, it must be considered that the TEM plan view technique allows observing only the superficial layer of the sample due to the thinning procedure that completely removes the substrate and the innermost part of the deposited film. To investigate the structure through the entire thickness, cross sectional TEM observations were also performed (Fig. 4(a–c)). Comparing the three different samples one can observe that the upper part of the films is very similar in terms of lateral grain dimension and separation among grains, as already observed in the plan view images (Fig. 3(a–c)). On the contrary, different microstructural features can be observed in films with different thickness. All the samples can be considered as formed by an initial thin layer at the interface with the Ru underlayer, consisting of nanograins physically in contact among them; on top of such layer, well separated columnar islands grow, whose height increases with increasing thickness, with an intergrain distance remaining roughly constant through the entire film thickness (Fig. 4(c)).

Such peculiar microstructural features are expected to strongly influence the magnetization reversal mechanism, in particular because the relative importance of the columnar vs. quasi-continuous morphology changes with the thickness. To study in detail the magnetization reversal mechanism, angular and time dependent measurements as well as numerical micromagnetic simulations were carried out.

3.2. Magnetic properties

Room temperature perpendicular and in-plane hysteresis loops are shown in Fig. 5(a–c). All samples exhibit a strong perpendicular magnetic anisotropy although a weak in-plane (hard axis) hysteretic

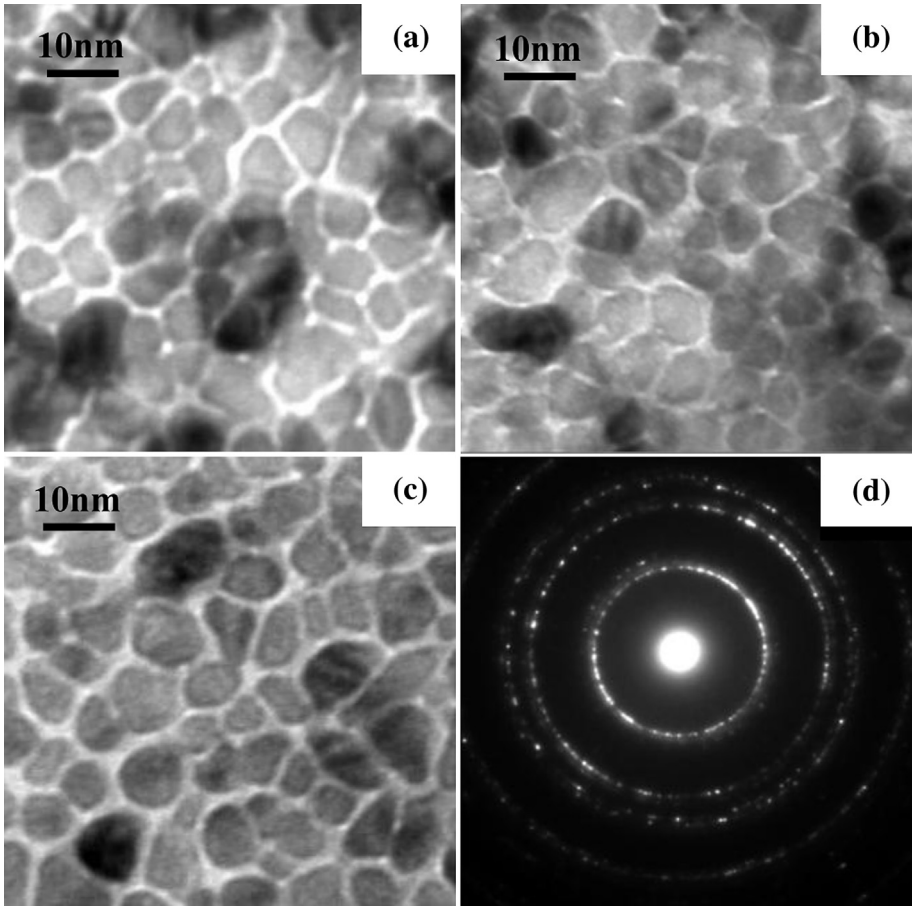

Fig. 3. TEM plan view of samples ML7.5 (a), ML10 (b) and ML17.5 (c). The selected area electron diffraction (SAED) pattern of the sample ML17.5 is reported in (d).

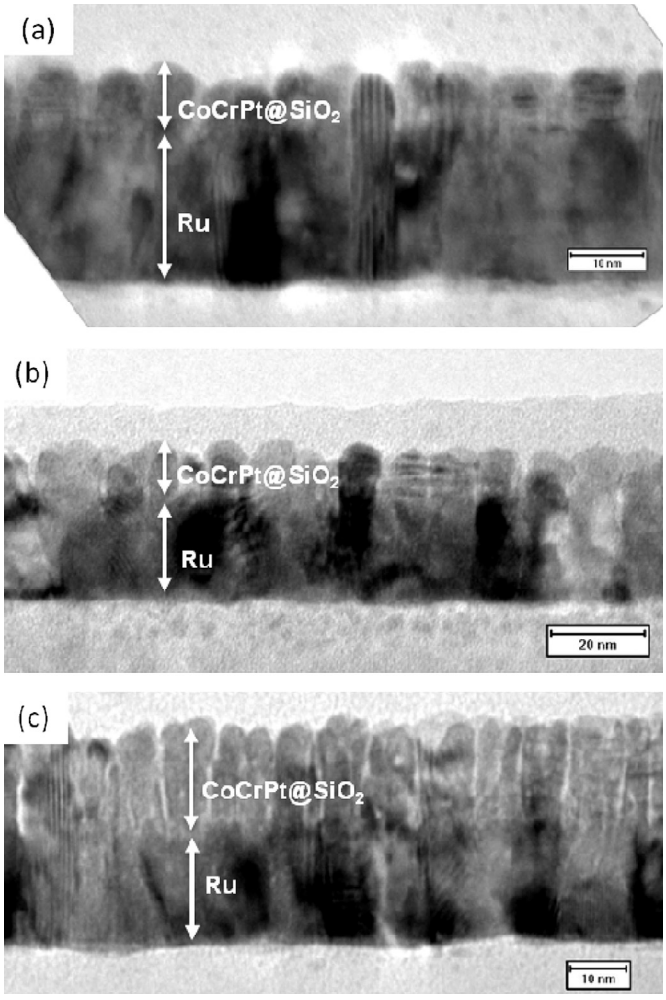

Fig. 4. TEM cross section of samples ML7.5 (a), ML10 (b) and ML17.5 (c).

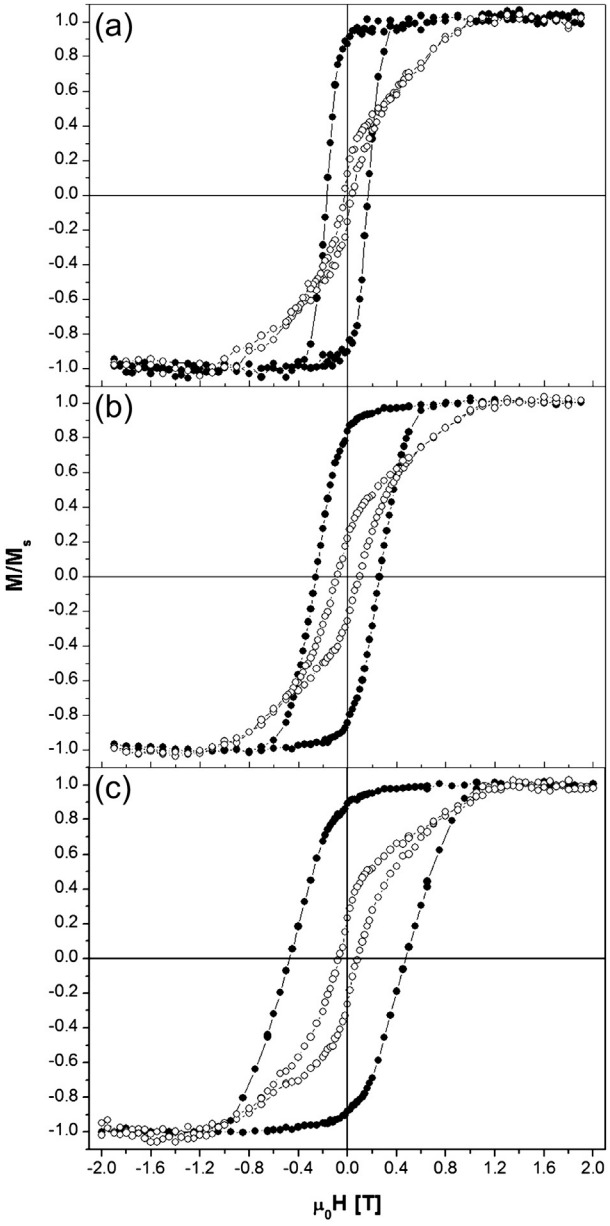

Fig. 5. Normalized (M/M_s) perpendicular (– ● –) and in-plane (– ○ –) magnetization loops at room temperature for samples ML7.5 (a), ML10 (b) and ML17.5 (c).

contribution is also present because of the angular dispersion of the easy axis (*c*-axis), as indicated by the structural analysis.

To enable a comparison among the films, the values of perpendicular coercivity ($H_{c,\perp}$), reduced remanence ($M_{r,\perp}/M_s$) and coercive squareness $S^* = 1 - M_{r,\perp}/\alpha H_{c,\perp}$ (where α is the hysteresis slope at coercivity) were evaluated and are summarized in Table 3 together with the values of the saturation magnetization M_s and the effective anisotropy constant expressed as $K_{\text{eff}} = \mu_0 H_k M_s/2$, where H_k is the anisotropy field estimated as the field where the in-plane magnetization (hard axis direction) and perpendicular magnetization curves merge.

K_{eff} and $M_{r,\perp}/M_s$ do not change significantly with increasing the magnetic layer thickness, with values of $\sim 5–6 \cdot 10^5$ J m^{-3} and ~ 0.85, respectively; in contrast, $H_{c,\perp}$ and S^* strongly depend on the magnetic layer thickness: $\mu_0 H_{c,\perp}$ increases from (170 ± 5) mT to (475 ± 5) mT and S^* decreases from (0.49 ± 0.01) to (0.17 ± 0.01) with increasing thickness. The reduction of both coercivity and coercive squareness with increasing magnetic layer thickness, indicates that, overall, the intergranular exchange coupling, which promotes cooperative reversal, progressively reduces. This is related to the non-uniform microstructure developing along the film thickness as evidenced by the TEM analysis (Fig. 4); in particular, on increasing the thickness, the relative importance of the region with well separated islands raises, leading to a decrease of exchange coupling among grains.

Information on the magnetisation reversal was derived by measuring at room temperature the angular dependence of the switching field (H_{sw} vs. ϕ), where ϕ is the angle between the applied field H and the easy axis EA, as defined in the inset of Fig. 6(a) and comparing the results with the theoretical Stoner–Wohlfarth (SW) [13] and Kondorsky [14] models (Fig. 6(b)). The Kondorsky model describes the magnetic reversal of continuous as well as of highly exchange-coupled films by domain wall motion (incoherent switching). In our case of nanogranular films with an average grains size of 7 nm, the existence of domain walls can be related to the formation of magnetic domains involving a number of individual grains, termed "interaction domains" [15,16]; in such a case the magnetic reversal can be controlled by expansion of the interaction domains and the movement of domain walls. On the other hand, in the SW model, the magnetization reversal of a single, isolated and uniaxial particle/grain occurs through coherent

Table 3
Main magnetic parameters obtained from the analysis of the perpendicular and in-plane hysteresis loops.

ID sample	M_s [MA m^{-1}]	K_{eff} [10^5 J m^{-3}]	$M_{r,\perp}/M_s$	$\mu_0 H_{c,\perp}$ [mT]	S^*
ML7.5	0.88 ± 0.03	4.8 ± 0.2	0.86 ± 0.02	170 ± 5	0.49 ± 0.01
ML10	0.84 ± 0.03	5.3 ± 0.3	0.84 ± 0.02	255 ± 5	0.27 ± 0.01
ML17.5	0.88 ± 0.03	5.7 ± 0.3	0.88 ± 0.02	475 ± 5	0.17 ± 0.01

rotation of the magnetization vector. This model can be applied to highly oriented particulate media and non-interacting granular films.

The angular dependence of the switching field was determined by measuring at different ϕ values, a series of the so-called easy axis DCD curves (*Direct Current Demagnetization curves*) by using the following non-conventional procedure [17]: first, a negative saturating field is applied along the easy axis, then the field is reduced to zero and the magnet is rotated to an angle ϕ from the initial position. In such a way, the initial magnetization state is the remanent state along the easy axis direction. Starting from an initial applied field of 20 T (and without further rotation) the so-called easy axis remanent magnetization (M_{re}) is measured along the easy axis direction after each reversing field application until the maximum positive field is reached. This procedure is then repeated for different values of ϕ. From each easy axis DCD curve, the remanence coercivity H_r (defined as the point where the remanence is zero) is determined. According to [17], the so-deduced H_r is more appropriate to investigate the switching process with respect to the remanence coercivity evaluated by using the conventional procedure where the DCD curves are collected along the field direction. Indeed, when the conventional procedure is used, H_r is equal to the switching field H_{sw} only along the easy axis, whereas at other ϕ angles, H_r and H_{sw} are not necessarily equivalent. On the other hand, when the non-conventional procedure is adopted, the equivalence between H_r and H_{sw} is expected at each ϕ angle. The easy axis DCD curves of the sample ML17.5 are shown in Fig. 6(a), whereas in Fig. 6(b) the angular dependence of H_{sw} of all samples, normalized to the switching field along the easy axis ($H_{sw,0^\circ}$), is reported together with the theoretical Stoner–Wohlfarth and Kondorsky switching curves.

Coherent and incoherent reversal processes coexist in all the samples and the degree of coherence enhances with increasing magnetic layer thickness, as indicated by the depth of the minimum at 45° which reaches the lowest value ($H_{sw,45^\circ}/H_{sw,0^\circ} = 0.76$) for the thickest film. These results are consistent with the non-uniform microstructure, which develops along the film thickness. Incoherent switching behaviour is due to the initial layer consisting of grains in close contact; the increasing portion of the region with well separated grains enhances the coherent behaviour with the increase of magnetic layer thickness.

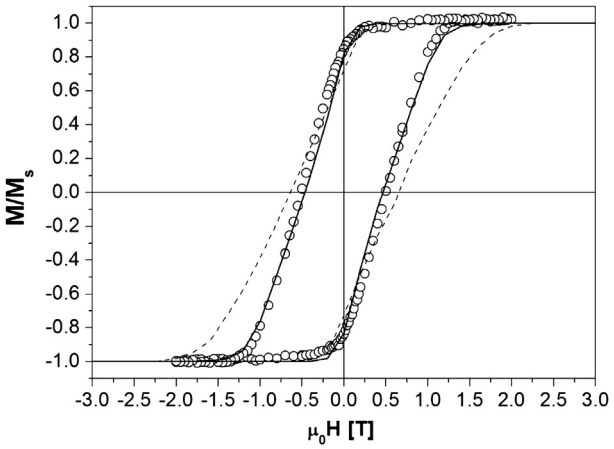

Fig. 7. Numerical micromagnetic simulation of room temperature hysteresis loops for sample ML17.5. – ○ –: experimental data. Continuous line: simulated curve with parameter $A_{int} = (0.7 \pm 0.1)\cdot 10^{-11}$ J m^{-1} and $K = (5.5 \pm 0.5)\cdot 10^5$ J m^{-3}; dotted line: simulated curve with parameters $A_{int} = 0$ and $K = (5.5 \pm 0.5)\cdot 10^5$ J m^{-3}.

It can be noted that numerical simulation of perpendicular hysteresis loops of samples ML17.5 (Fig. 7) well reproduces the experimental findings, taking into account a finite level of intergrain exchange coupling (A_{int}), lower than the bulk exchange constant ($A_{bulk} \sim 1\cdot 10^{-11}$ J m^{-1}), even in this sample. Indeed, the simulated loop for a CoCrPt film with fully exchange decoupled grains ($A_{int} = 0$; dotted line in Fig. 7) shows larger coercivity values and loop closure at fields higher than the experimentally observed values.

To confirm the analysis, the effect of thermal activation on the switching process was also taken into account. Indeed, the experimental data were collected at a finite temperature, while the two theoretical switching models apply at zero temperature. This aspect was investigated for sample ML17.5, which presents the strongest coherent switching character. A series of remanence curves were measured using field waiting times t between 10 and 1000 s by applying the reverse field (for t seconds) along three different ϕ angles (0°, 45° and 90°) and measuring the moment along the easy axis direction (Fig. 8(a)). From each of these curves the switching

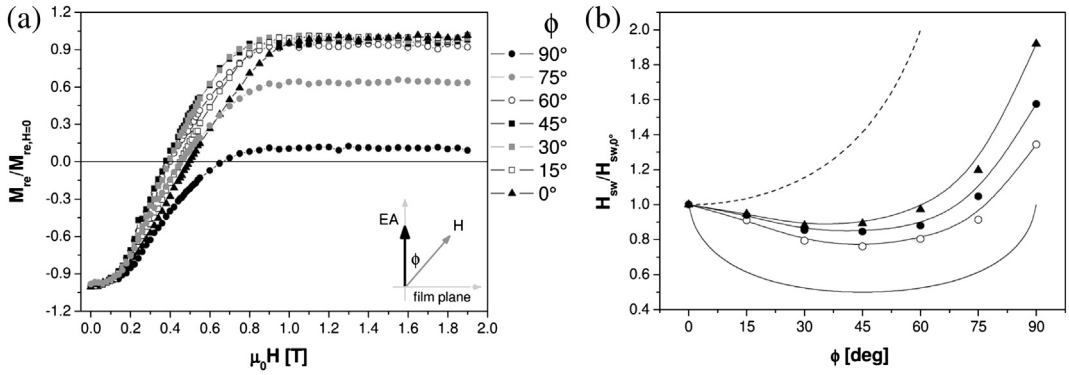

Fig. 6. (a) Room temperature normalized ($M_{re}/M_{re,H=0}$) easy axis DCD curves of samples ML17.5 collected with the field applied along different ϕ angles with respect to the sample easy axis EA (inset). (b) Angular dependence of the normalized switching field ($H_{sw}/H_{sw,0^\circ}$) of samples ML7.5 (– ▲ –), ML10 (– ● –) and ML17.5 (– ○ –); the theoretical Stoner–Wohlfarth (continuous line) and Kondorsky (dashed line) switching models are also reported.

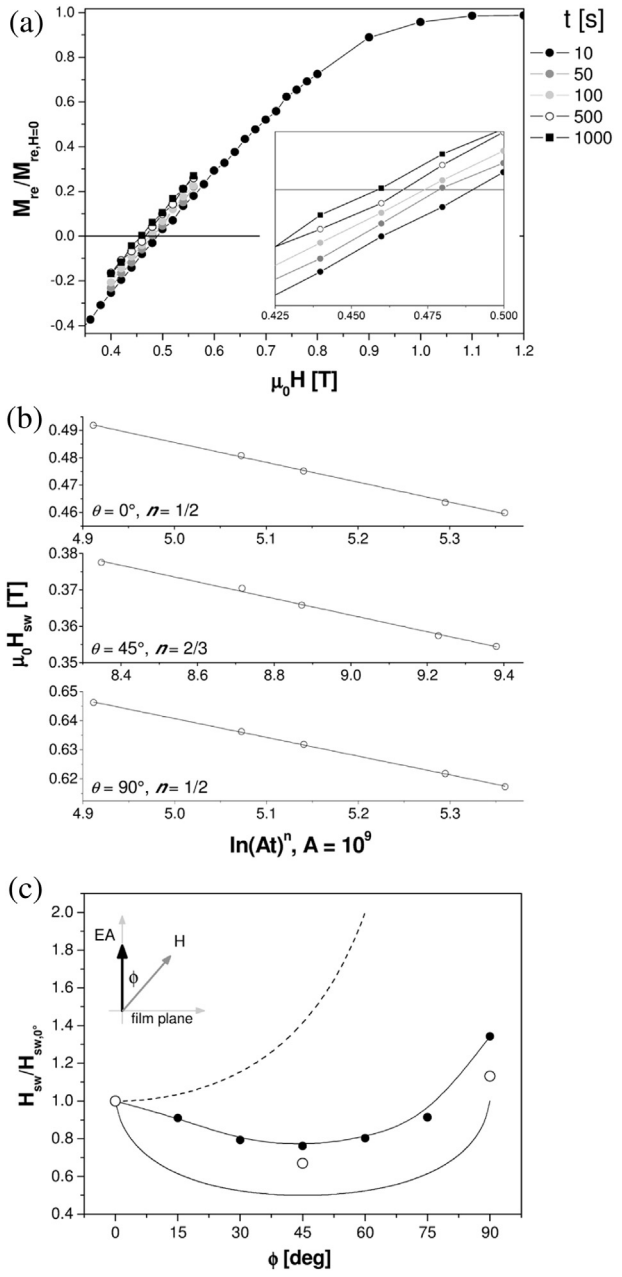

Fig. 8. Sample ML17.5 – (a) Room temperature easy axis remanence curves measured along the film normal for different field waiting times ($10 < t < 1000$ s); inset: magnification of the curves around $H_r \equiv H_{sw}$. (b) Time dependence of H_{sw} measured at three different ϕ angles: 0°, 45° and 90°. (c) Angular dependence of the normalized switching field ($H_{sw}/H_{sw,0°}$) before (– ● –) and after (– ○ –) correction for the thermal effects; the theoretical Stoner–Wohlfarth (continuous line) and Kondorsky (dashed line) switching models are also reported.

field values ($\equiv H_r$) were extracted and plotted as a function of the waiting time in Fig. 8(b). Then, the experimental data were fitted with the Sharrock's equation [18] in order to obtain by extrapolation the time independent switching parameter H_{sw0} (i.e. the switching field at 0 K):

$$H_{sw}(\phi, t) = H_{sw0}(\phi)\left\{1 - \left[\frac{k_B T}{KV}\ln(At)\right]^n\right\} \quad (1)$$

where A is the frequency factor (assumed to be 10^9 Hz), k_B is the Boltzmann constant, T is the absolute temperature and V is the volume where the magnetization reversal occurs. The value of n is dependent on the orientation of the anisotropy axis and it is set at 1/2 for $\phi = 0°$ and 90°, and at 2/3 for $\phi = 45°$, being the reversal mechanism of the sample ML17.5 prevalently Stoner–Wohlfarth like [18]. The switching fields at 0 K (H_{sw0}) and 300 K (normalized to the switching field along the easy axis, $H_{sw,0°}$) are shown in Fig. 8(c): the shape of the two curves are quite similar revealing a further reduction of $H_{sw0,45°}/H_{sw0,0°} = 0.67$ after the correction, indicating that the reversal mechanism of the investigated samples is essentially the same arising from the analysis of the room temperature angular dependence of the switching field.

The gradual reduction of the intergrain exchange coupling with increasing the magnetic layer thickness is expected to affect the activation volume v_{act}, which is defined as the smallest unit reversing its magnetization. Due to the perpendicular anisotropy of the films, in order to compensate for the self-demagnetization fields, the activation volume was evaluated by using the waiting time method proposed in Ref. [19]. By this method it is possible to determine the fluctuation field H_f which is a fictitious field representing the coupling of the thermal fluctuations with the magnetic moment:

$$H_f \cong -\left.\frac{\partial H}{\partial \ln(t)}\right|_{M_{irr}} \quad (2)$$

from this field, v_{act} can be determined by using the following equation:

$$v_{act} \sim \frac{k_B T}{\mu_0 H_f M_s} \quad (3)$$

According to Equation (2), H_f can be determined from time-dependent measurements of the irreversible magnetization M_{irr} at different reversing field increments. Then, at constant M_{irr} value,

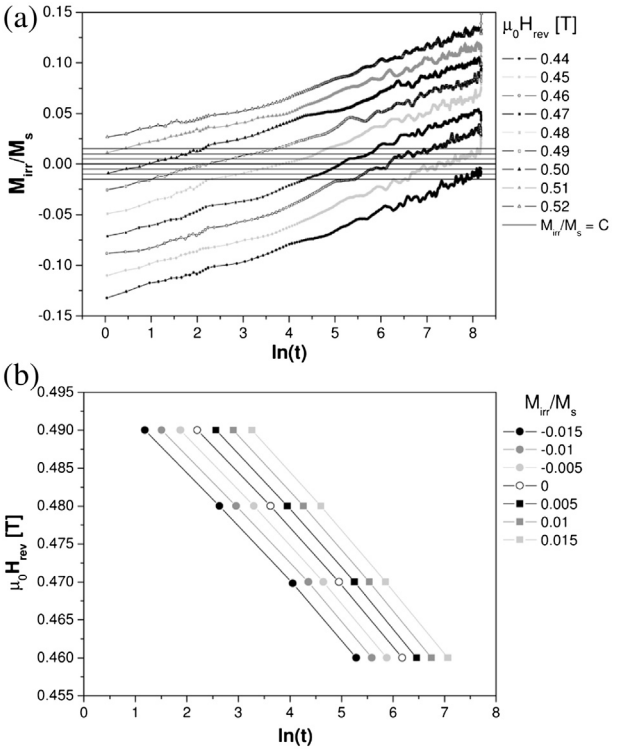

Fig. 9. Sample ML17.5 – (a) Family of M_{irr} vs. ln(t) curves measured at room temperature for different reversing fields H ranging between 4.4 and 5.2 kOe; the M_{irr}/M_s = Const lines are reported ($C = 0, \pm 0.005, \pm 0.01, \pm 0.015$). (b) Family of H vs. ln(t) at different values of M_{irr}/M_s around the remanence coercivity (i.e. $M_{irr}/M_s = 0$).

Table 4
Comparison between the average values of activation volume v_{act} and physical volume V_{gr} of the cylindrical grains (diameter = 7 nm, height = th).

ID sample	v_{act} [nm^3]	V_{gr} [nm^3]	v_{act}/V_{gr}
ML7.5	650 ± 60	300 ± 10	2.15
ML10	660 ± 60	350 ± 10	1.90
ML17.5	620 ± 60	660 ± 10	0.95

plots of H vs. ln(t) will be linear and the slope of the variation gives H_f. Since the measurement of the fluctuation field is made at a constant value of the magnetization, the demagnetizing fields are constant and H_f can be determined independently.

The magnetization decay was measured along the film normal by using the following procedure: initially, the sample was magnetically saturated along the easy axis and then a reversing field H was applied in the opposite direction; the subsequent change of the total magnetization M_{tot} was measured over a period (t) of 3600 s in presence of different reversing fields around the switching field. The data were corrected for the reversible component of magnetization using the DCD method where the time dependent irreversible magnetization is $M_{irr}(H,t) = M_{tot}(H,t) - M_{rev}(H)$ (t = 3 s) [20]. For sample ML17.5, a family of M_{irr}/M_s vs. ln(t) curves measured at different reversing fields is reported in Fig. 9(a). According to the waiting time method, these curves can be used to directly calculate H_f at a certain constant magnetization level. For example, at the remanence coercivity (i.e. $M_{irr}/M_s = 0$), a line is drawn and the data point (H,t) where the time dependent curve intersects with the line is obtained. The trend of the applied reversing field as a function of ln(t) is reported in Fig. 9(b) for different values of M_{irr}/M_s around the remanence coercivity (i.e. $M_{irr}/M_s = 0$). The data in Fig. 9(b) indicate that H is linear with ln(t) which is consistent with Equation (2). From the slope of these curves the average value of H_f around the switching field, which is connected to the v_{act} through Equation (3), was determined. The values of v_{act} and physical volume V_{gr} of the cylindrical grains are compared in Table 4. As the magnetic layer thickness increases, the v_{act}/V_{gr} ratio decreases because of the gradual reduction of the intergrain exchange coupling.

4. Summary and conclusions

The correlation between the microstructure and magnetization reversal mechanism was investigated as a function of thickness in granular CoCrPt:SiO_2 films with perpendicular magnetic anisotropy.

TEM plane view and cross section analysis indicate the development of a non-uniform grain isolation along the film thickness: an initial layer consisting of nanograins physically in contact among them forms at the interface with the Ru underlayer; on top of such layer, well separated columnar grains (7 nm average size) grow, whose height increases with increasing thickness, with an intergrain distance remaining roughly constant through the entire film thickness. The increasing relative importance of the region with well separated islands leads to a decrease of exchange coupling among grains.

This non-uniform microstructure was found to strongly influence the magnetization reversal mechanism. The analysis of angular and time-dependent magnetic measurements results indicates that the magnetization reversal mechanism is determined by the coexistence of coherent and incoherent processes, with a tendency towards more coherent reversal processes (i.e. Stoner–Wohlfarth character) as the thickness of the magnetic layer increases. The change in the predominant reversal mechanism is coherent with the observed reduction of the v_{act}/V_{gr} ratio (activation volume v_{act} and physical volume V_{gr} of the grains) with the increase of thickness.

Acknowledgements

The authors thank E. Patrizi for technical assistance in magnetic measurements. This work was financially supported by the European Commission FP7 project TERAMAGSTOR (contract N. FP7-ICT-2007-2-224001).

References

[1] H.J. Richter, J. Phys. D Appl. Phys. 40 (2007) R149.
[2] S.N. Piramanayagam, in: S.N. Piramanayagam, T.C. Chong (Eds.), Developments in Data Storage: Materials Perspective, John Wiley & Sons, Inc., Hoboken, NJ, USA, 2011.
[3] V. Sokalski, D.E. Laughlin, J.-G. Zhu, Appl. Phys. Lett. 95 (2009) 102507.
[4] Y. Inaba, T. Shimatsu, T. Oikawa, H. Sato, H. Aoi, H. Muraoka, Y. Nakamura, IEEE Trans. Magn. 40 (2004) 2486.
[5] M. Zheng, B.R. Acharya, G. Choe, J.N. Zhou, Z.D. Yang, E.N. Abarra, K.E. Johnson, IEEE Trans. Magn. 40 (2004) 2498.
[6] S.N. Piramanayagam, C.K. Pock, L. Lu, C.Y. Ong, J.Z. Shi, C.S. Mah, Appl. Phys. Lett. 89 (2006) 162504.
[7] K. Srinivasan, S.N. Piramanayagam, R.W. Chantrell, Y.S. Kay, J. Magn. Magn. Mater. 320 (2008) 3036.
[8] H.S. Jung, M. Kuo, S.S. Malhotra, G. Bertero, Appl. Phys. Lett. 91 (2007) 212502.
[9] H.S. Jung, U. Kwon, M. Kuo, E.M.T. Velu, S.S. Malhotra, W. Jiang, G. Bertero, IEEE Trans. Magn. 43 (2007) 615.
[10] http://llgmicro.home.mindspring.com.
[11] K. Srinivasan, S.N. Piramanayagam, R. Sbiaa, R.W. Chantrell, J. Magn. Magn. Mater. 320 (2008) 3041.
[12] LEPTOS 3.03, Bruker AXS, Germany.
[13] E.C. Stoner, E.P. Wohlfarth, IEEE Trans. Magn. 27 (1991) 3475.
[14] E. Kondorsky, J. Phys. 2 (1940) 161.
[15] W. Rave, D. Eckert, R. Schafer, B. Gebel, K.-H. Muller, IEEE Trans. Magn. 32 (1996) 4362.
[16] R.K. Mishra, R.W. Lee, Appl. Phys. Lett. 48 (1986) 733.
[17] K.R. Coffey, T. Thomson, J.U. Thiele, J. Appl. Phys. 92 (2002) 4553.
[18] M.P. Sharrock, J. Appl. Phys. 76 (1994) 6413.
[19] M. El-Hilo, K. O'Grady, R.W. Chantrell, J. Magn. Magn. Mater. 248 (2002) 360.
[20] D.C. Crew, S.H. Farrant, P.G. McCormick, R. Street, J. Magn. Magn. Mater. 163 (1996) 299.